



Strathprints Institutional Repository

Ewing, Helen and Hendry, Alan and Nash, David (2011) *Finite element analysis applied to redesign of submerged entry nozzles for steelmaking*. Proceedings of the Institution of Mechanical Engineers, Part L: Journal of Materials: Design and Applications, 225 (4). pp. 327-339. ISSN 1464-4207

Strathprints is designed to allow users to access the research output of the University of Strathclyde. Copyright © and Moral Rights for the papers on this site are retained by the individual authors and/or other copyright owners. You may not engage in further distribution of the material for any profitmaking activities or any commercial gain. You may freely distribute both the url (<http://strathprints.strath.ac.uk/>) and the content of this paper for research or study, educational, or not-for-profit purposes without prior permission or charge.

Any correspondence concerning this service should be sent to Strathprints administrator: <mailto:strathprints@strath.ac.uk>

Finite Element Analysis Applied to Redesign
of Submerged Entry Nozzles for Steelmaking

H.C. Ewing^{a,*}, A. Hendry^a, D.H. Nash^a,

^aDepartment of Mechanical Engineering, University of Strathclyde, 75 Montrose St,
Glasgow, G1 1XJ, UK

Abstract

The production of steel by continuous casting is facilitated by the use of refractory hollow-ware components. A critical component in this process is the submerged entry nozzle (SEN). The normal operating conditions of the SEN are arduous, involving large temperature gradients and exposure to mechanical forces arising from the flow of molten steel; experimental development of the components is challenging in so hazardous an environment. The effects of the thermal stress conditions in relation to a well-trying design were therefore simulated using a finite element analysis approach. It was concluded from analyses that failures of the type being experienced are caused by the large temperature gradient within the nozzle. The analyses pointed towards a supported shoulder area of the nozzle being most vulnerable to failure and practical in-service experience confirmed this.

As a direct consequence of the investigation, design modifications, incorporating changes to both the internal geometry and to the nature of the intermediate support material, were implemented, thereby substantially reducing the stresses within the Al₂O₃/graphite ceramic liner. Industrial trials of this modified design established that the component reliability would be significantly improved and the design has now been implemented in series production.

Keywords: finite element; thermal stress; refractory; submerged entry nozzle; continuous casting; steelmaking; design; alumina graphite.

1 INTRODUCTION

1.1 Refractory Components in Steelmaking

The function of refractory components in the continuous casting of steel is two-fold. First, the liquid steel must be contained, directed and introduced into the casting mould in a controlled manner. Modern casting involves pouring a number of ladles of steel in a continuous sequence which requires the establishment of a reservoir of liquid and the ability to change ceramic components if necessary during the casting sequence, Fig. 1. The second function of the refractory nozzles is to protect the liquid steel flow from the possibility of oxidation by air during casting which would result in unacceptable levels of oxide inclusions in the steel. The life of such nozzles is invariably short, typically on the order of some hundreds of minutes [1].

Until now the design of refractory pouring tubes has largely evolved from an empirical approach which combines in-service experience of the users with the knowledge built up in various ceramic manufacturing companies. In general, this has been an adequate, if not optimal, mode of development but, nevertheless, it is recognised in the industry that hollow-ware operates very close to the limit of performance and that small, seemingly insignificant, changes, either in the design or manufacture of the refractory component, or in operating procedure in the steel works, can lead to failure in service. Such failures are almost invariably catastrophic, leading to spillage of liquid steel, and are extremely expensive in loss of time and product as a full casting sequence is interrupted. The refractories used in ladle shrouds and

submerged entry nozzles are based on oxide ceramic and flake graphite materials. The mixture of materials is chosen to be mechanically strong, to have high thermal conductivity, and to resist erosion/corrosion by the flow of liquid steel. The tubes are manufactured by cold isostatic pressing, followed by pressureless sintering in a controlled atmosphere. The resulting product is a porous ceramic which is fitted with metallic parts to allow for argon gas purging of the assembly in service, and to facilitate attachment of the nozzle to tube-changer mechanisms. Within this complex component, it is, however, possible to devise improvements based on the application of new design methods and the use of improved materials which could significantly increase the margin of safety and the economy of use. Until now, progress in implementing new approaches has been somewhat inhibited due to the innate conservatism in the industry which arises from very obvious safety considerations. Hitherto, new materials or design concepts have been introduced by an empirical approach, traditional in the refractories industry, but the advent of rapid, cost effective finite element analysis offers the opportunity to assess potential improvements due to changes in design or materials of refractory components more safely and economically than has previously been the case.

The specific objective of the present work, then, was to develop a finite element model to improve the design and manufacture of pouring tubes (refractory hollow-ware); the approach developed here can also be applied more widely to the design of ceramic ware in other similar operating environments. The particular pouring tube examined was the submerged entry nozzle which is used to convey molten steel on its way from the tundish to the mould as depicted in Fig. 1. In service, the risk of thermal shock to the SENs, at the start of the pouring sequence, is minimised by pre-heating

the component to 500°C, but SENs must also endure large steady state temperature gradients, with temperatures ranging from approximately 1500°C at the bore, in contact with the molten steel, whilst the air temperature outside the tube section is 200°C.

As already stated, steel breakouts due to SEN failures can be extremely dangerous and as a result the approach to experimental design changes has been risk-averse. The operating environment is not conducive to any form of experimental stress analysis method. It is clear, then, that the problem is rather intractable with regard to engineering development. It is for these reasons that finite element analysis has the potential to be an attractive tool for evaluating the performance of new design configurations and, given the ability to tailor the properties of refractory materials in practice, to determine optimal materials properties to minimise stress within the SEN.

1.2 Computational Analysis of Refractory Components

A number of reports have described recent applications of finite element analysis in relation to thermal and structural investigations of refractories in steelmaking and continuous casting. These have tended to concentrate around problems relating to the pouring ladle and its shroud (e.g., [2, 3]) and furnace linings, such as in basic oxygen furnaces [4]. Yoshikawa et al stated that there has been little stress analysis work done on multilayer SENs [5] and, in relation to design analysis, this continues to be the case. Schmitt et al used the case of the submerged entry nozzle to demonstrate the efficacy of applying a combined micromechanics/computational approach to prediction of the microstructural performance of the alumina/graphite material under conditions of thermal shock [6]. In a similar sense, Deng et al used finite element

analysis of microstructure to develop a regime for inducing residual stresses during the SEN manufacturing process with the aim of reducing erosion of the component in service [7]. However, given that the present work was aimed directly at using the thermal and structural analysis capabilities of finite element analysis to improve the performance of an existing SEN design within the constraints imposed by geometry and cost, coupled with the need to use a standard range of materials, then perhaps the most encouraging report was by Raidl [8]; in this, he stated that by using computational thermal and mechanical analysis in the redesign of the refractories of vacuum degassing components in steelmaking, and with no change to the constituent materials, the life of the equipment was extended in service by 100%.

2. ASSESSMENT OF ORIGINAL SEN DESIGN

2.1 Description

The submerged entry nozzle comprises a ceramic liner at the bore, housed in a steel casing with a layer of insulating cement between. Fig. 2 shows a typical head section of an SEN. The ceramic material is a mixture of Al_2O_3 and graphite flake, the graphite being added to increase the thermal conductivity of the material, thereby improving the component's resistance to thermal stress and thermal shock. The choice of material used in the bore of the nozzle is critical to the purity of the produced steel because dissolution of refractory components into the molten steel can lead to an undesirable level of contamination of the product. The nozzles are submerged throughout the casting process in order to prevent oxidation of the liquid metal and the steel exits the SEN through two ports on opposite sides of the pouring tube, as illustrated in Fig. 3.

2.2 Numerical Analysis Procedure

The commercial finite element package, ANSYS (Version 12) [9], was used in the present work. In the first instance, a coupled thermal stress analysis was used to identify regions of high stress of the original SEN configuration, leading dimensions of which are given in Fig. 3. The geometry of the SENs is symmetrical about 2 axes and therefore it was necessary to generate only a quarter-model of the geometry and apply symmetry boundary conditions to the nodes lying on the faces parallel to the axes of symmetry. The upper 150 mm of the SEN was modelled, as failures occur only within this head section.

2.3 Thermal Analysis Elements

For the thermal analysis, the component was modelled using the ANSYS SOLID 87 element; this is a 3-dimensional 10 node tetrahedral thermal solid element, which can be conveniently utilised to describe curved geometries. The element has a single degree of freedom, temperature, at each of its 10 nodes. A default element size of 10mm was employed in all the analyses reported here, as this was found to provide a suitable compromise between accuracy and solution time. Front and rear views of the quarter-geometry mesh of the original configuration are shown in Fig. 4. (At this stage of the investigation, it was decided that, primarily with regard to speed of computation, the interfaces between the constituent components of the SEN would be shared. As will be demonstrated, the considerable attractions of this approach regarding its convenience of application are negated by its results.)

The temperature of the molten steel, which was applied to the nodes at the bore, was 1500°C, whilst the air temperature surrounding the SEN was measured in service to be 200°C.

The overall heat transfer coefficient, needed to enable the finite element analysis to compute the local rate of heat dissipation from the surface of the SEN, was obtained using an iterative procedure described in the flow chart, Fig. 5. First of all, the heat transfer coefficient by free convection (h_c) over a vertical cylinder in a turbulent air flow was taken to be 12.7 watts/m²K [10] and can be assumed to be virtually constant over the surface and fluid temperature range of interest in the current problem. For a thermally radiating surface, the heat radiated, Q_r , is given approximately by the Stefan-Boltzmann Law:

$$Q_r = \varepsilon\sigma T^4 \quad (1)$$

where ε = the surface emissivity = 0.8 for oxidised steel [11], σ = the Stefan-Boltzmann constant = 56.7×10^{-12} kW/m²°K⁴ and T = surface temperature °K.

Following the procedure shown in Fig 5, a value of surface temperature of 500°C, known to be the pre-heated temperature of the SEN and the approximate value in service over much of the uniform cylindrical area of the assembly, was used to “seed” the process. The radiation component, h_r , of the heat transfer coefficient (outer surface to surroundings) was iteratively modified until the surface temperature, T_{FE} , obtained from the finite element heat transfer simulation of the conduction *through the SEN wall*, equalled the surface temperature, T_{cr} , computed from predictions of heat transfer *away from the surface* by combined free convection and radiation. Using this approach, the value for the total heat transfer coefficient, h_{total} , converged to 41

watts/m² °K. This value, used throughout the work, together with the thermal properties of the materials given in Table 1 [11] allowed the steady state temperature profile across the SEN to be determined by finite element thermal analysis.

2.4 Structural Analysis Elements

The elements used at this stage in the structural analysis were ANSYS SOLID 92; this element is a 3-D 10-node tetrahedral structural solid element. In this element, three degrees of freedom exist at each node: translations in the nodal x, y and z directions. The nodal temperature values from the thermal analysis were imported into the structural analysis model. The structural solver was then able to compute the distribution of stresses arising from the imposed temperature condition.

In service, the SEN is supported under two parallel shoulders by equi-spaced springs, numbering three on each side. In order to apply this support in the model, the nodes under two parallel shoulders were fully constrained in the vertical (i.e., y) direction, this representing the worst case. The springs under the shoulders exert an upwards force on the SEN such that its top surface is pressed against the slide gates above (the gates are used to control the flow of steel into the nozzle). This condition was represented in the models by fully constraining the nodes at the top surface in all directions.

2.5 Preliminary Results – Thermal Load

In order to set a baseline for the subsequent study, the original “in-service” design of the SEN was first analysed with the aim of examining whether the large temperature gradient alone is sufficient to cause failure. Fig. 6(a) shows the computed temperature

distribution throughout the entire SEN. The peak temperature difference across the SEN is seen to be 890°C, as the temperature of the outer surface of the steel casing is 610°C compared with 1500°C at the bore. Fig. 6(b) shows the temperature profile within the Al₂O₃/graphite ceramic material in isolation, this being the component of primary concern. It can be seen that a large temperature gradient exists across the Al₂O₃/graphite ceramic material, 1500°C at the bore and 883°C at the outermost edge of the ceramic at the top surface.

As previously stated, the temperature distribution computed in the initial stage of the analysis was imposed on the structural model to produce a stress distribution. Contours of 1st principal stress magnitude are shown in Fig. 7. The Rankine failure criterion was employed [13], this being suitable for low cohesion materials typified by the brittle Al₂O₃/graphite ceramic under investigation, and which states that failure occurs when the maximum principal stress reaches the uniaxial tensile strength of the material. The failure criterion was set to 10 MPa, the Modulus of Rupture (MOR) of the Al₂O₃/graphite ceramic material [12]. The lower and upper limits of the stress plot contours were set to 1 MPa and 10 MPa respectively, to allow low stress and high stress critical regions to be easily identified.

Based on this analysis, the stresses within the Al₂O₃/graphite would be predicted to be in excess of the critical limit of 10 MPa throughout most of the SEN body, as can be seen in Fig. 7 and very little variation was observed between the bulk of the supported and the unsupported shoulder (right hand and left hand shoulders respectively in Fig. 7).

The observations above lead to a conclusion that the effects of standard operating temperatures would be very much more than sufficient, invariably, to cause the SEN to fail when, in fact, it is known from practical experience that this is not the case. In the model, the three sections of the SEN, the ceramic, the insulating cement and the steel casing, are joined together by common interfaces comprising shared nodes. This representation means that thermal expansion of each individual material must also be accommodated by the adjoining materials. So, for example, the steel casing at the outer surface, which the model predicts to experience a temperature of 610°C, will undergo far greater displacement, due to thermal expansion, than the insulating cement and the ceramic material, owing to the higher thermal expansion coefficient of the steel, Table 1. As a consequence, the contiguous insulation concrete and ceramic materials are displaced unrealistically by their attachment to the steel casing, resulting in unfeasibly large tensile forces within the head section of the SEN.

Further, the top surface nodes of the component are fully constrained in the x, y and z directions and therefore expansion upwards is not permitted in the model. This constraint prevents displacement of the top of the ceramic, of the insulating cement, and of the steel casing sections. Each of these experiences thermal expansion which generates tensile forces within the critical head section of the SEN.

The maximum stress, 221 MPa, was observed along the edge of the base of the supported shoulder at the rear of the SEN. This effect can also be attributed to the constraints imposed upon the component by the model, which have been shown to be unrealistic. The shoulder support is represented in the model by fully constraining the surface nodes under the shoulder in the y direction. This constraint prevents

expansion in the vertical direction at the shoulder region. Expansion in the head section of the supported shoulder region can therefore only be accommodated in the outward radial direction, owing to the combined vertical constraint on the top surface and on the base of the shoulder. This condition generates large tensile stresses at the shoulder constraint as the nodes in this region are constraining the effects of the thermal expansion in the vertical direction.

3. ENHANCED MULTI-COMPONENT MODEL

3.1 Limitations of Simple Model

The use of shared interfaces, within the simple model, between each of the three different materials of the SEN (ceramic, insulating cement and steel), and full constraint at the top surface, led to a prediction of unrealistically high stress. A more representative simulation was developed by reconfiguring the model of the SEN into a multi component assembly. Each component of the SEN was now modelled as an entirely separate geometric entity, each having a separate interface connected to the neighbouring component indirectly by contact elements. The top surface constraint was also removed and replaced with contact elements connected to additional volumes which were designed to represent the slide gate above the SEN.

3.2 Analysis Procedure – Multi-Component SEN Assembly

In this approach, the interfaces between the components consisted of two sets of nodes at identical locations. As the SEN geometry was no longer a continuous body, it was necessary to couple the two sets of nodes at each of the interfaces with respect to temperature. In other words, the model enabled heat flow by direct conduction through the ceramic-concrete and concrete-steel interfaces.

The inclusion of contact elements at the interfaces provided the three components comprising the SEN with limited constraint insofar as penetration of one interface through the surface of the adjoining component is prevented. The contact and target elements used in all the contact analysis in the present work were ANSYS CONTA 174, a 3-D, 8 node, surface-to-surface contact element used to represent contact and sliding between 3D target surfaces defined by target elements, TARGE 170. CONTA 174 has 3 degrees of freedom at each node: translations in the nodal x, y and z directions. The contact elements are located on the surfaces of the 3-D structural elements, these being of identical type to those used in the simple preliminary model.

At the ceramic-concrete interface, the ceramic surfaces were defined as the contact surface and the concrete areas as the target (towards which the contact surface moves in this type of analysis). The contact type was set to 'standard' for the ceramic-concrete interface, this setting permitting both sliding and separation (it was evident from post-service examination of these nozzles that separation does, in fact, occur at this interface). Likewise, for the concrete-steel interface the concrete areas were defined as the 'contact' surface and the steel areas as 'target', with the contact type set to 'sliding'. The coefficient of friction for each solid interface is given in Table 2 [14, 15]. The temperature distribution of the thermal analysis was imported into the structural analysis where it was used to calculate thermal stress.

The model was developed further by the inclusion of volumes above the top surface of the SEN to represent the slide gate. A mirror image of the top surface was created and these areas were then translated upward to form 30 mm deep volumes. The slide

gate volumes extend 5 mm beyond the edge of the SEN in the model to allow for SEN expansion. Contact elements were included at the interface between the top of the three SEN components and the slide gate. The areas at the top surface of the SEN were defined as the contact surface and the areas at the base of the slide gate were designated as the target surface, the target and contact elements utilised being as detailed above. The contact type was set as 'standard' and the coefficients of friction are given in Table 2. The volumes representing the slide gates were fully constrained in the x, y and z directions and omitted from the thermal solution.

4. Results

This multi-component model of the SEN incorporating interfacial contact elements was solved using identical thermal parameters to those used in the earlier, simple, shared-interface model so as to allow direct comparison of the two solutions, and to enable examination of the influence of the model boundary conditions.

The steady state temperature profiles obtained for both the simple single entity model and for the multi-component contact model for the original SEN design are almost identical and this is as one would expect. The thermal gradient across the ceramic is 1500 – 883°C in the simple model, and 1500 – 885°C in the multi-component contact model. (Similar temperature profiles are to be expected as the additional volumes representing the slide gate are not included in the thermal solution and heat conduction through the body in the enhanced model is represented by thermally coupling the nodes at the interfaces.)

4.1 Differences between analytical predictions

There are considerable differences between the stress distribution generated by the effect of temperature within the $\text{Al}_2\text{O}_3/\text{graphite}$ material in the simple model (Fig. 7) and that of the multi-component contact model (Fig. 8). In the enhanced analysis model, the tensile stress induced throughout the major part of the entire body of the $\text{Al}_2\text{O}_3/\text{graphite}$ ceramic, with the exception of some higher stress regions at the transition between the head section and the tube section at the rear of the SEN, is below the failure criterion of 10 MPa. (Extended in-service experience of operation of this configuration of SEN confirms that the unit is, in fact susceptible to failure in the zones highlighted by the enhanced model, as will be discussed below.)

In the simple model, high tensile stresses (max 221 MPa) are present in the head section and close to the bore on both the supported and unsupported sides of the $\text{Al}_2\text{O}_3/\text{graphite}$ ceramic material (right and left hand side respectively in Fig. 7). In the enhanced model, however, the unsupported edge of the $\text{Al}_2\text{O}_3/\text{graphite}$ ceramic is under compression at the bore region, whilst the supported shoulder experiences tension at the bore and compression in the upper head section above the shoulder support (Fig. 8). These differences are due to the respective boundary conditions.

4.2 Interpretation of computed results

The large differences in predicted stress distribution between the two different modelling approaches can be explained as follows. In the simple model the top surface nodes are fully constrained, preventing any displacement of the component, and the different materials comprising the SEN are joined at shared interfaces. The large temperature gradient across the component, 1500°C at the bore and 610°C at the outer casing, causes the SEN materials to expand and the joined interfaces force the

ceramic material to be displaced unrealistically, generating high tensile stresses throughout the SEN in the simple model. The inclusion of contact elements at the materials interfaces in the enhanced model, although greatly increasing the computational cost of analysis (by about three orders of magnitude), provides greater confidence in the veracity of the model and reduces the predicted tensile stresses to levels which operational experience confirms are generally sustainable, albeit with a degree of variability in component life. Confidence in the enhanced model was further reinforced by the observation that, employing the Rankine failure criterion to the stress plots, the zone predicted to have the highest tensile values of principal stress was located in the area in which failures in this particular type of SEN invariably occur (Fig. 8) [12].

5. SEN Design Modification

One of the primary objectives of the work reported here was to establish which factors were responsible for the mode of failure frequently observed in an existing design of SEN. The insight gained from the analysis was next put to use in a radical redesign of the unit which was modified by removing the brittle Al_2O_3 /graphite material from the shoulder section and the stress raising corner area. The outer dimensions of the steel casing could not be altered as these are dictated by the practical configuration of the steel plant fixtures and it was desirable to retain the Al_2O_3 /graphite material at the bore to exploit the advantageous properties of the material i.e., excellent resistance to erosion and corrosion. However, it was possible to alter the geometry of the ceramic component within these restrictions by replacing the Al_2O_3 /graphite at the shoulder with refractory concrete and contouring the Al_2O_3 /graphite ceramic to remove any abrupt changes in geometry which could potentially act as stress raisers. An iterative

process of geometric modification led to an optimised final geometry of improved design as shown in Fig. 9.

Analysis of the improved design was conducted using identical parameters and boundary conditions to those previously described for the original in-service design in the enhanced (with contact interfaces) numerical model. Fig. 9 shows the meshed quarter geometry of the final iteration of improved design.

Fig. 10 shows front and rear views of the 1st principal stress profile in the Al₂O₃/graphite material of the final improved geometry. The stress throughout the upper section of the Al₂O₃/graphite ceramic is everywhere well below the critical limit of 10 MPa, and a maximum of only 3.2 MPa is predicted, a substantial decrease when compared to the original design, ($\sigma_{I \max} = 39$ MPa). Furthermore, there is a large area under compressive stress close to the bore in both the supported and unsupported shoulders of the Al₂O₃/graphite ceramic; this will substantially eliminate crack movement towards the bore, and provides confidence that the modified design will be much less vulnerable to this mode of failure than was the original design.

A further advantage of the new design is that there is a decrease in the temperature gradient across the Al₂O₃/graphite ceramic. In the original design, the temperature difference was computed to be 615°C at the top surface of the Al₂O₃/graphite ceramic, as shown in Fig. 6(b). However, in the modified design the difference falls by approx. 50% to 274°C, as the temperature of the outer surface of the ceramic is increased to 1226°C as a result of the design modifications (Fig. 12). In addition to the predicted consequence of this, in the reduction in steady-state thermal stress, it is likely to be

beneficial in reducing the transient effects of thermal shock to the component on start up.

5. Discussion - General

The results of the multi component contact analyses of the original design suggest that the steady-state thermal conditions alone are sufficient locally to initiate component failure. The tensile stress, within the component head around the supported shoulder, exceeds the failure criterion of the Al₂O₃/graphite material only in a localised area. Operational experience confirms that failures invariably stem from cracks originating in the area highlighted by the analysis. These results are in line with post-service observations of failed SENs of the original configuration, which invariably show that the failure crack initiates at the change in section of the supported shoulder and propagates upwards at an angle of 45° towards the bore [12].

Looking in more detail at the original design, one can see that the supported shoulder is more severely affected by the stress generated by the high temperatures, as shown in Fig. 8. However, in the unsupported shoulder, a region of compression at the bore serves to inhibit crack propagation and protect the shoulder.

5.1 Discussion - Implementation of Design Improvements

The analyses performed here provided valuable insights and directed modifications to the design of the SEN. It appeared that removal of the weak Al₂O₃/graphite ceramic material from the vulnerable shoulder regions of the SEN would prove beneficial in reducing the stress within the Al₂O₃/graphite material to below the failure criterion of 10 MPa.

Further, in the modified design, the Al_2O_3 /graphite material surrounding the bore region is now computationally predicted to be in compression, the objective in this regard being to improve resistance of the SEN to the initiation and growth of cracks.

Having predicted, from the finite element analyses, that the modified design would experience tensile stress within the Al_2O_3 /graphite ceramic section of the SEN well below the failure criterion, this design was taken forward to trial. These were successful and the reliability of the component has been significantly enhanced, resulting in very worthwhile concomitant gains in plant availability and safety. The design has now been adopted into series production [12].

6. Conclusions

Finite element analysis of this type of complex problem, that of a submerged entry nozzle for continuous steel casting, involving, as it does, large temperature differences, steep temperature gradients, stress loadings, and a mixture of components with widely varying material properties, has been shown to be a practicable and efficient tool for design development.

It was established that a simple approach to the analysis, in which the components shared interfaces, resulted in a model which was over-constrained and, although desirable in terms of computational requirements, this approach predicted stress conditions which are known from experience to be unfeasible.

An enhanced solution strategy, in which the interface conditions were treated as contact problems, produced stress solutions which were in good agreement with the empirical evidence obtained from SENs which had failed in service. (No other experimental means of assessing the result was technically viable, given the aggressive environment of the in-plant conditions.)

Supported shoulders were found to be vulnerable to failure. By way of contrast, the corner under the unsupported shoulder is subjected to relatively low tensile stresses and, furthermore, the material immediately adjacent to this closer to the bore is also protected by being in compression.

Using the information revealed by the analysis, in conjunction with knowledge derived from practical operating experience of the original units, the task of devising an improved, more reliable design of SEN was simplified. Confidence in adopting the prototype units for trial operations was also reinforced by following this approach.

Subsequently, by applying this method of design analysis, it was possible conveniently to evaluate the performance of alternative candidate geometries. The result of this process indicated that replacement of the Al_2O_3 /graphite ceramic material in the vulnerable shoulder sections would reduce the tensile stresses in the component to less than 40% of the modulus of rupture.

Industrial trials of the modified design showed the component reliability to be greatly improved and the design has now been adopted as the manufacturer's standard product.

ACKNOWLEDGEMENTS

The authors gratefully acknowledge the support of the Engineering and Physical Sciences Research Council, RHI Refractories UK Ltd., and the use of ANSYS software made available through a faculty research licence by ANSYS Inc., Houston, PA.

REFERENCES

- [1] Mozherin, V.A., Sakulin, V.Y, Migal, V.P., Margishvilli, A.P., Konstantinov, A.A., Refractory objects and materials for continuous steel casting. *Refract. Ind. Ceram.*, 2008, **49**, 245-250
- [2] Li, S., Liu, Y., Yu, H., Three-dimensional thermo-mechanical finite element simulation for casting ladle structure under thermal loadings. *Mater. Sci. Forum*, 2008, **575-578**, 1-6.
- [3] Peruzzi, S., Glandus, J.C., Huger, M., Poirier, J., Numerical study of the in-service behaviour of refractory parts used in continuous casting, *Br. Ceram. Proc.*, 1999, **60**, 161-162.
- [4] Gruber, D., Andreev, K., Harmuth, H., Optimisation of the lining design of a BOF converter by finite element simulations, *Steel Res. Int.*, 2004, **75**, 455-461.
- [5] Yoshikawa, M., Ohtani, T., Ichikawa, K., Nakamura, R., Uchida, S., Evaluation of layer thickness to reduce the thermal stress in multilayer submerged nozzles, *Taikabutsu Overseas*, 1997, **18**, 25-29.
- [6] Schmitt, N., Burr, A., Berthaud, Y., Poirier, J., Micromechanics applied to the thermal shock behavior of refractory ceramics, *Mech. Mater.*, 2002, **34**, 725-747.

- [7] **Deng, J., Dongling, Y., Yuanqiang, T.**, Design, fabrication and performance of $\text{Al}_2\text{O}_3/(\text{W}_{0.7}\text{Ti}_{0.3})\text{C} + \text{Al}_2\text{O}_3/\text{TiC}$ multilayered ceramic nozzles, *Int. J. Refract. Met. Hard Mater.*, 2009, **27**, 734-739.
- [8] **Raidl, G.**, Analysis of heat and stress fields in RH degassers by means of finite element analysis, *I & SM*, 1991, **18**, 14.
- [9] ANSYS[®] Academic Research, Release 12, ANSYS Inc., Canonsburg, PA.
- [10] ESDU 77031, *Heat transfer by free convection and radiation – simply shaped bodies in air and other fluids*, (HIS ESDU Engineering Service, London).
- [11] **Cverna, F.**, *Thermal properties of metals*, 2002 (ASM International, Materials Park, OH).
- [12] **Lee, S.**, Private communication, RHI Refractories UK Ltd., Clydebank, Scotland.
- [13] **Pilkey, W.D., Dilkey, D.F.**, *Peterson's stress concentration factors*, 3rd edition, 2008 (John Wiley & Sons, Hoboken, NJ).
- [14] **Baltay, P., Gjelsvik, A.**, Coefficient of friction for steel on concrete at high normal stress, *J. Mater. Civil Eng.*, 1990, **2**, 46-49.
- [15] **Tassios T.P., Vintzeleou, E.N.**, Concrete-to-concrete friction, *J. Struct. Eng.-ASCE*, 1987, **113**, 832-849.

LIST OF FIGURE CAPTIONS

Fig. 1 Schematic illustrating continuous casting of steel

Fig. 2 Quarter section view of original SEN head

Fig. 3 Half section scale view of full length SEN

Fig. 4 Quarter section front and rear views of mesh of original configuration of SEN

Fig. 5 Flowchart showing method of iterative calculation of heat transfer coefficient

Fig. 6 Plot of computed temperature distribution throughout (a) all SEN components
(b) ceramic section in isolation, of the original design

Fig. 7 Front view of 1st principal stress distribution within the ceramic section of the original design, as predicted by the simple simulation

Fig. 8 Front and rear views of 1st principal stress distribution within the ceramic section of the original design, as predicted by the enhanced simulation including contact

Fig. 9 Quarter section view of modified SEN head

Fig. 10 Quarter section front and rear views of modified configuration of SEN mesh

Fig. 11 Front and rear views of 1st principal stress distribution within the ceramic section of the modified design, as predicted by the enhanced simulation including contact

Fig. 11 Plot of computed temperature distribution throughout (a) all SEN components
(b) ceramic section in isolation, of the modified design

APPENDIX

Notation

A_i	internal bore area
F	reaction force
g	universal gravitational constant
h	heat transfer coefficient
l	height of SEN
m	mass
MOR	modulus of rupture
Q	volumetric flow rate of liquid steel

Q_r	radiated heat
SEN	submerged entry nozzle
T	surface temperature
u	liquid steel velocity
ε	surface emissivity
ϕ_i	internal diameter of tube
ϕ_o	outer diameter of tube
μ	coefficient of friction
ρ	density of steel
σ	Stefan- Boltzmann constant
σ_1	1st principal stress

Table 1 Properties of materials used in SENS

Material	Density (kg / m ³)	Young's modulus (GPa)	Poissons ratio	Thermal conductivity (W. m ⁻¹ . K ⁻¹)	Thermal expansion (K ⁻¹)
Ceramic (Al ₂ O ₃ /graphite)	2380	2	0.25	13x10 ⁻⁶	4x10 ⁻⁶
Insulating cement	2000	15	0.3	1.2x10 ⁻⁶	7x10 ⁻⁶
Steel casing	7860	207	0.3	40x10 ⁻⁶	16x10 ⁻⁶
Refractory concrete	3100	30	0.3	3.1x10 ⁻⁶	7x10 ⁻⁶

Table 2 Coefficients of friction of contact interfaces used in enhanced model

Contact surface	Target surface	Coefficient of friction (μ)
Ceramic (Al_2O_3 /graphite)	Insulating cement (Refractory concrete in modified design)	0.65
Insulating cement (Refractory concrete in modified design)	Steel casing	0.47
Steel slide gate	Top surface of ceramic (Al_2O_3 /graphite)	0.47

Figure

[Click here to download high resolution image](#)

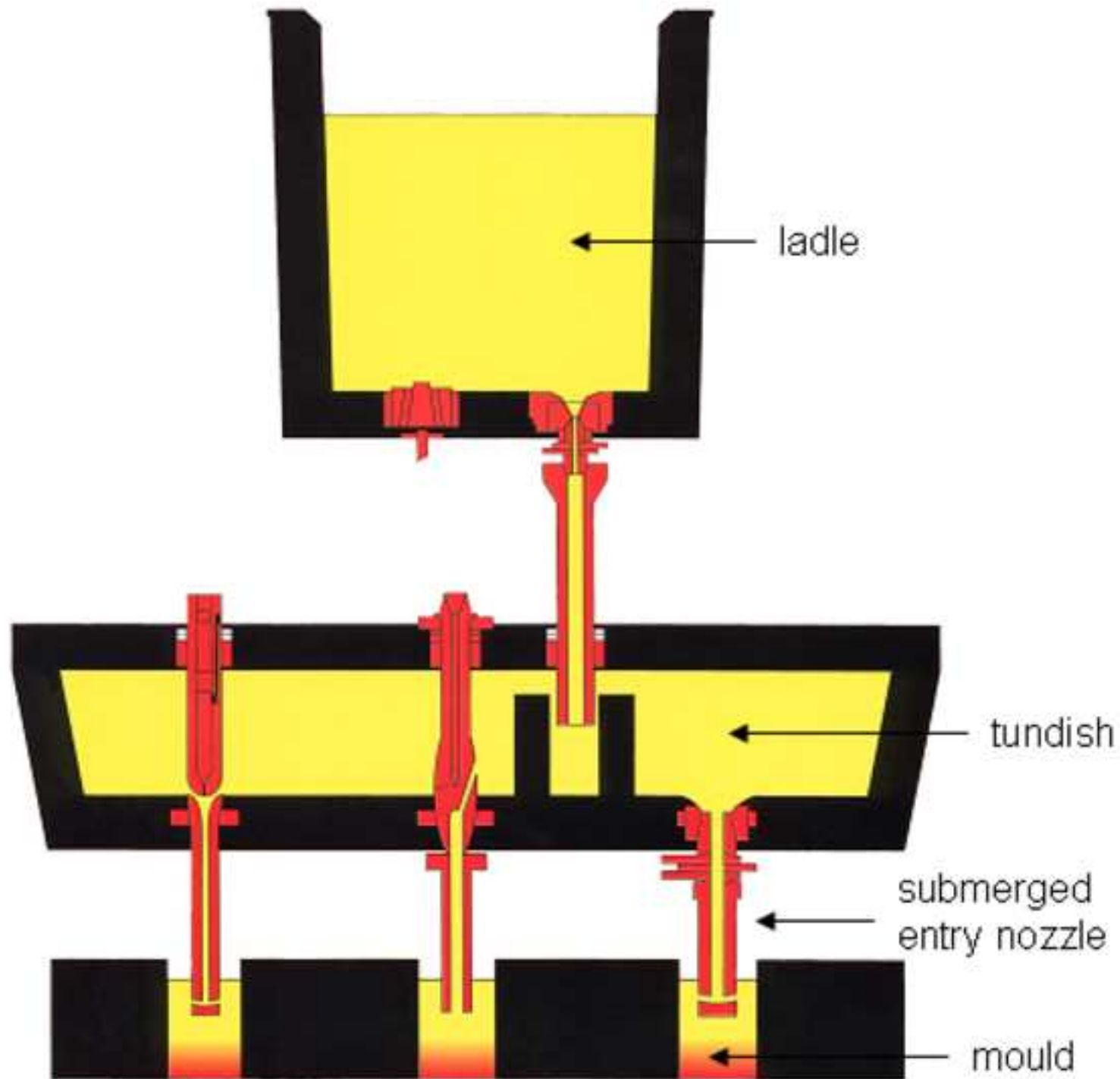
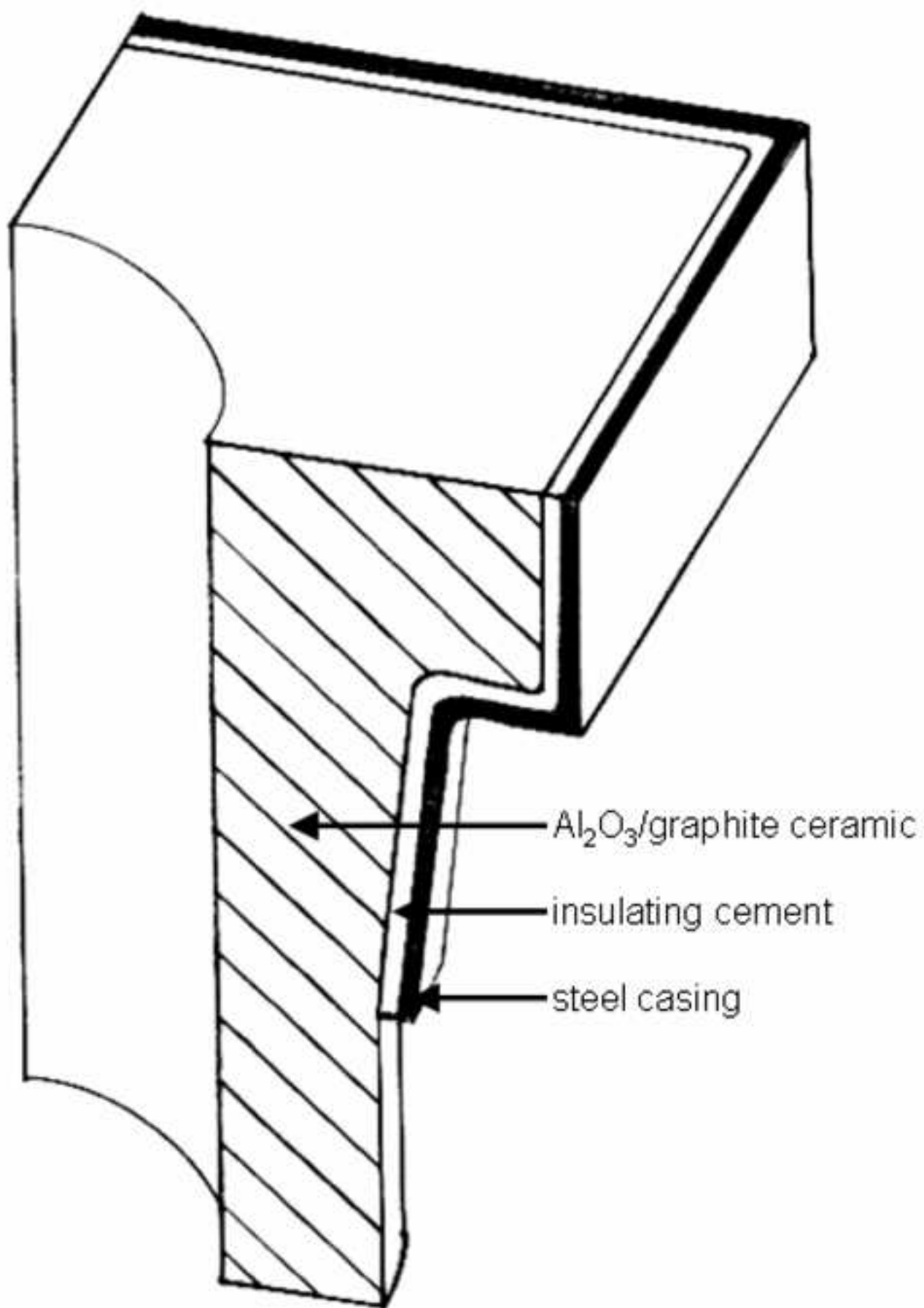
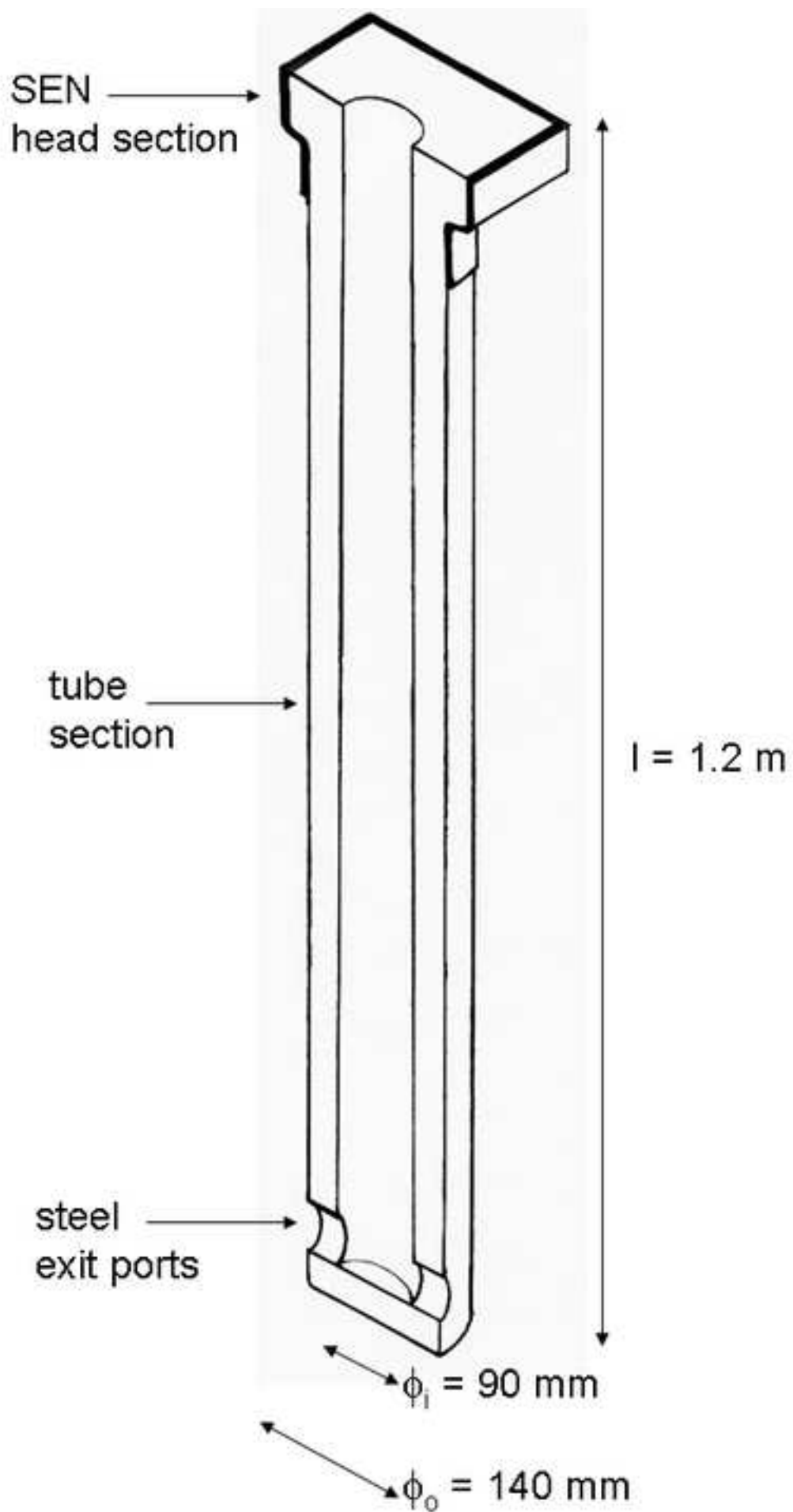


Figure
[Click here to download high resolution image](#)



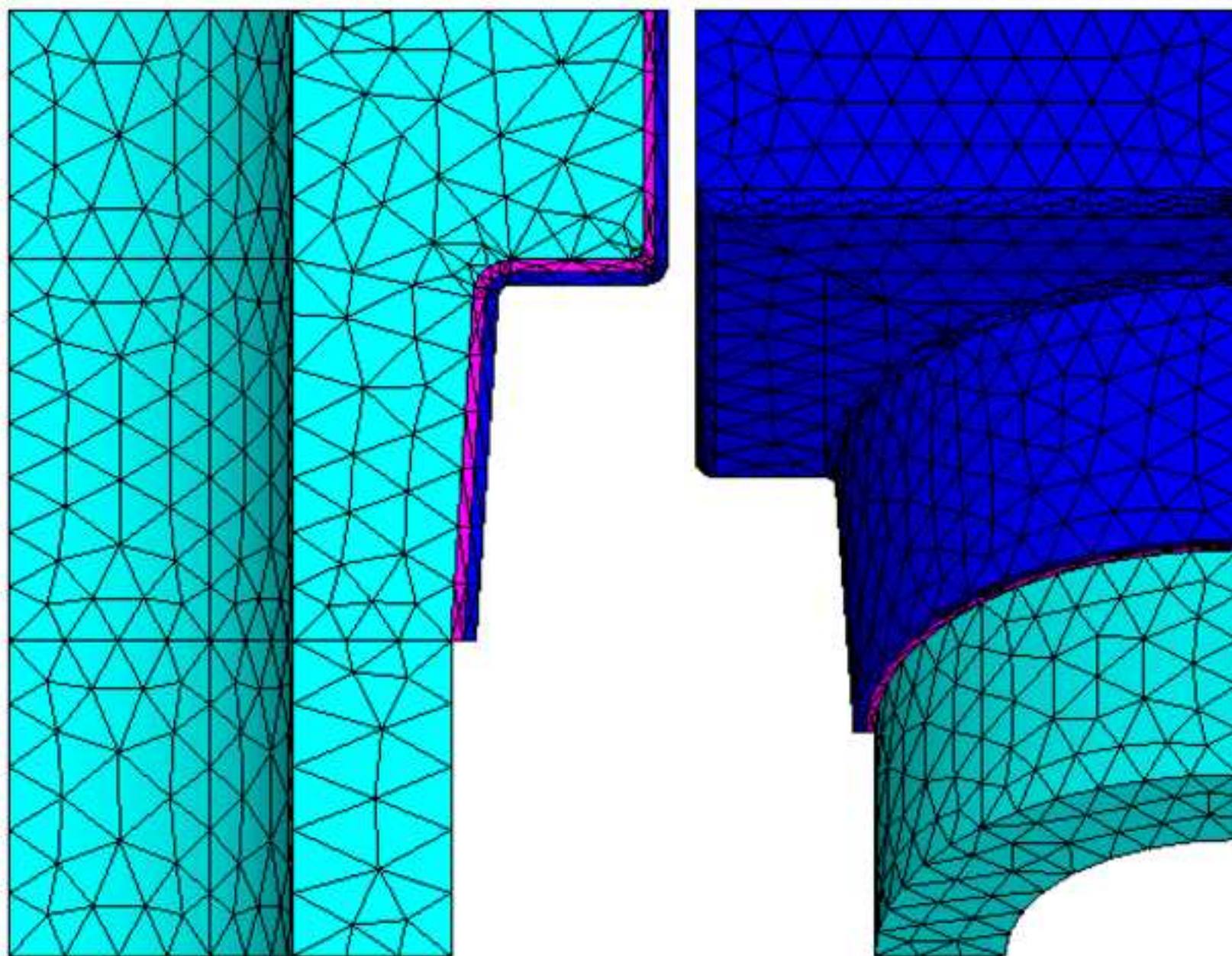
Figure


[Click here to download high resolution image](#)



Figure

[Click here to download high resolution image](#)



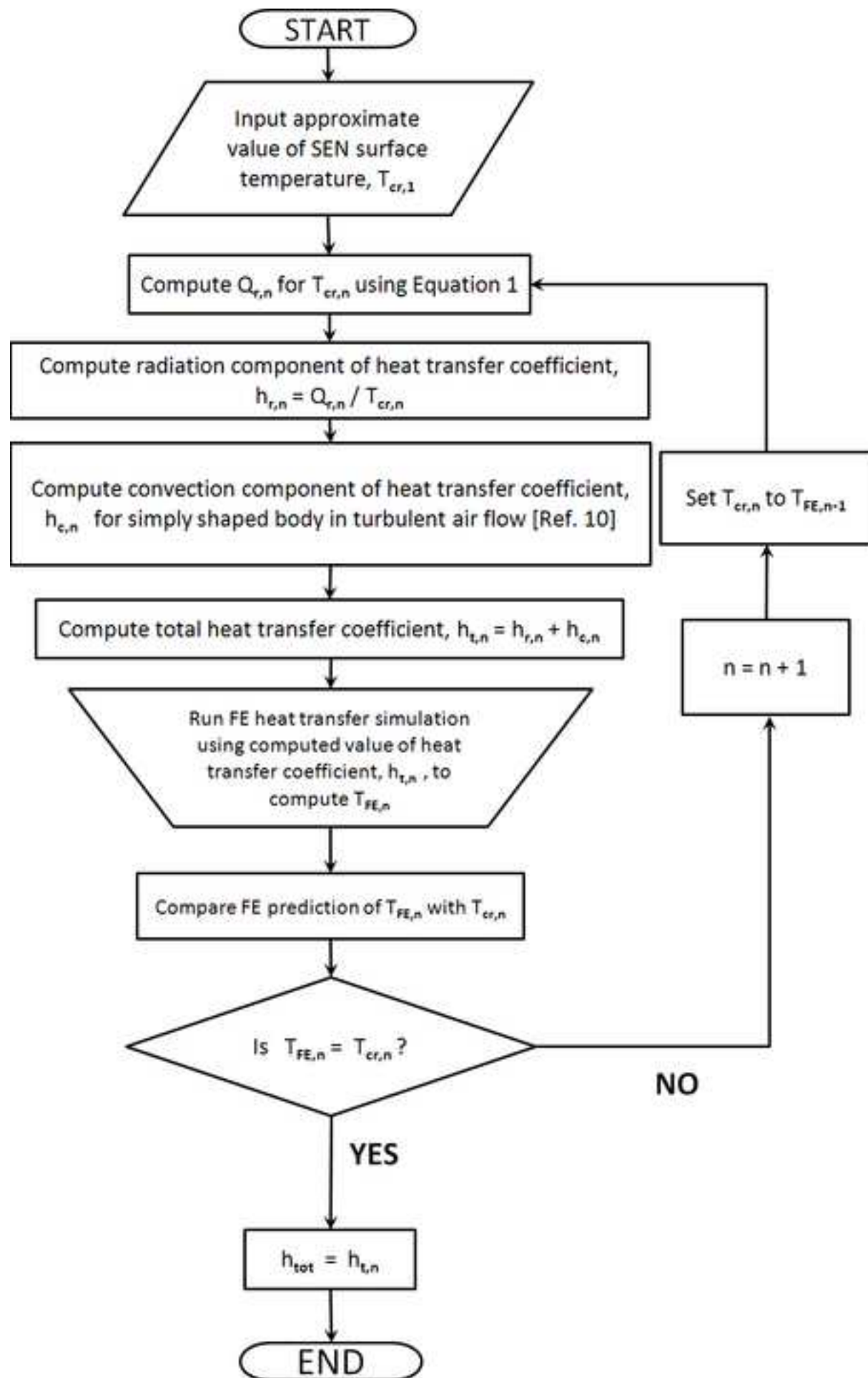
 Al_2O_3 /graphite ceramic

 insulating cement

 steel casing

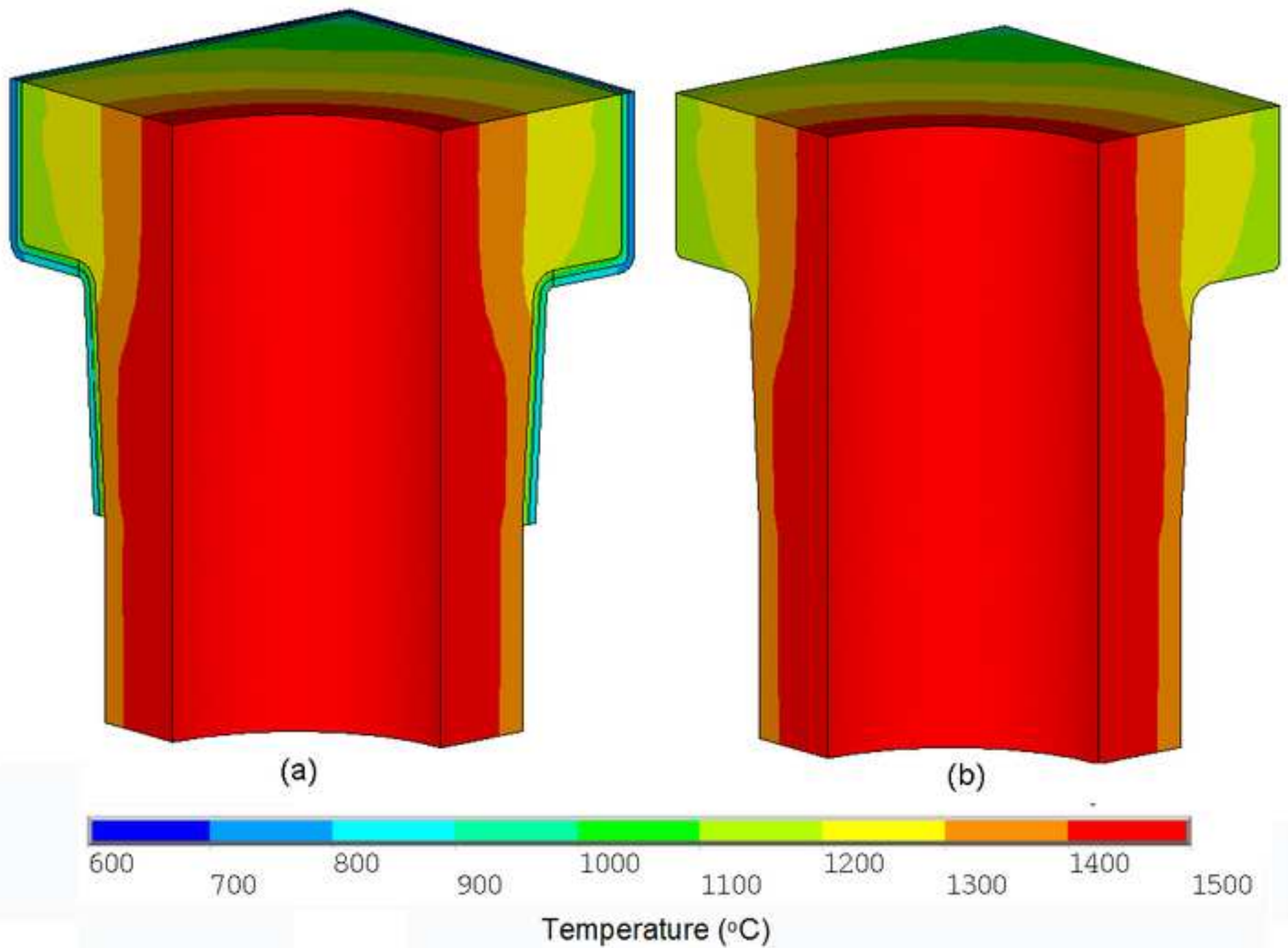
Figure

[Click here to download high resolution image](#)



Figure

[Click here to download high resolution image](#)



Figure

[Click here to download high resolution image](#)

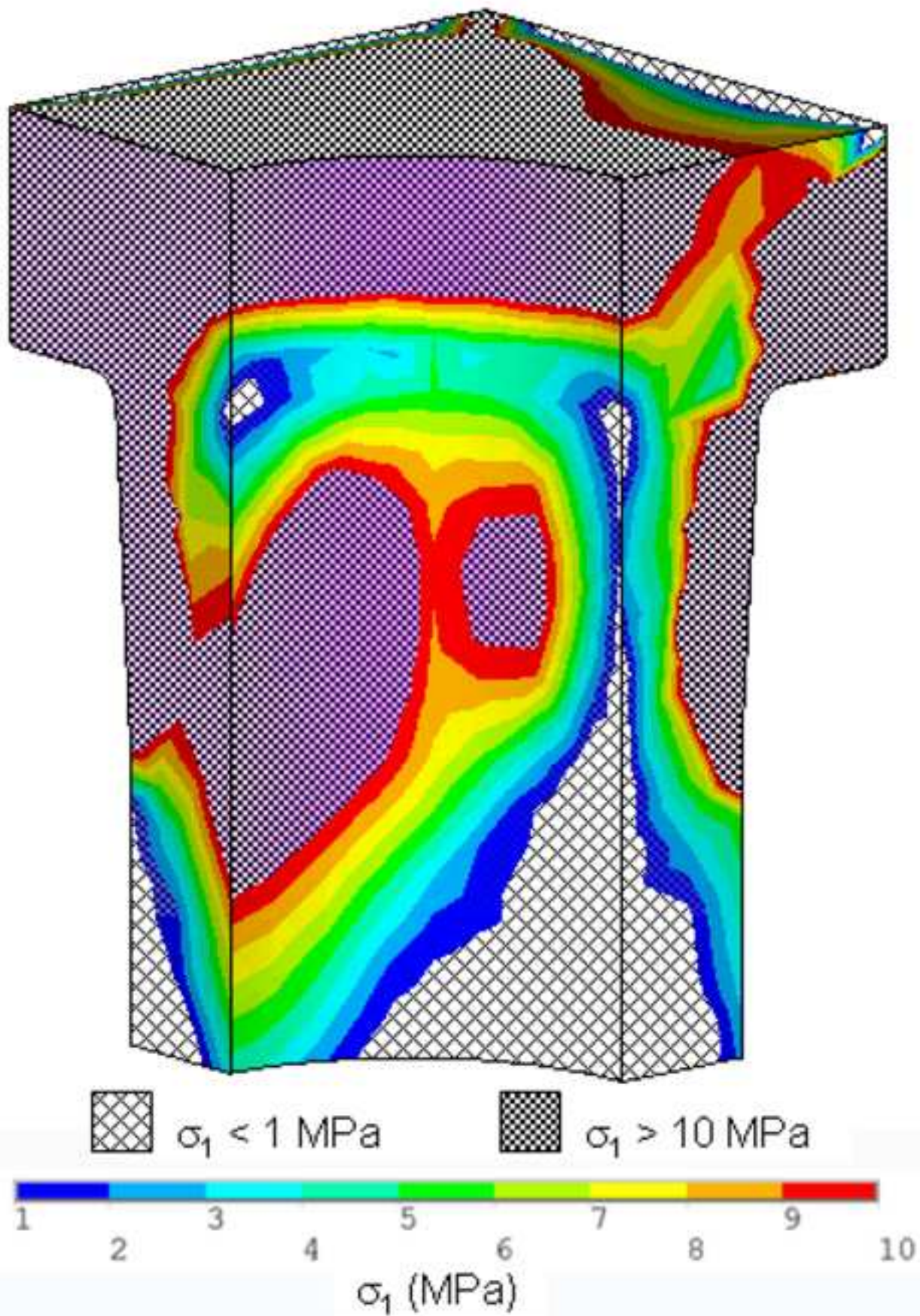


Figure
[Click here to download high resolution image](#)

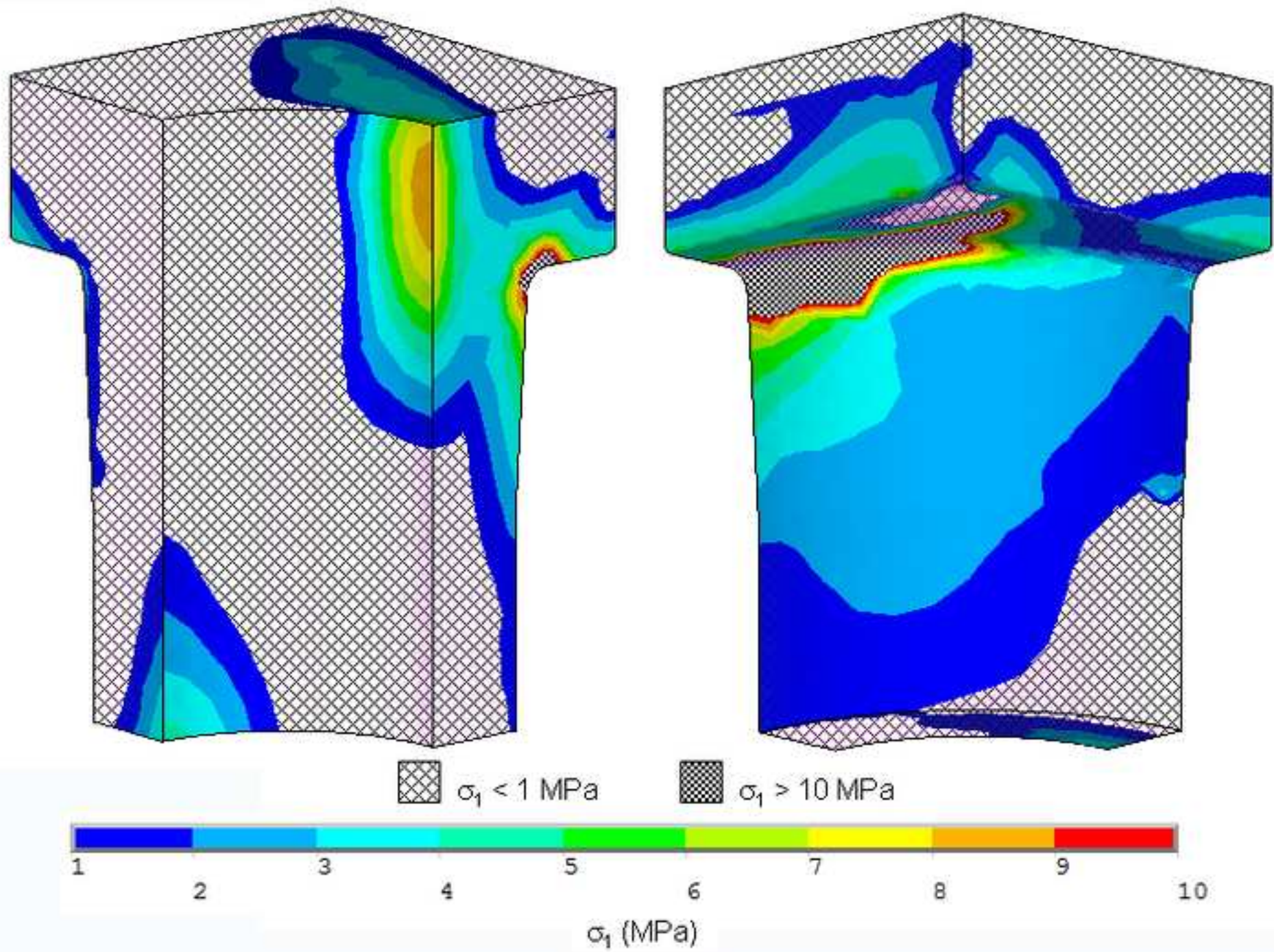
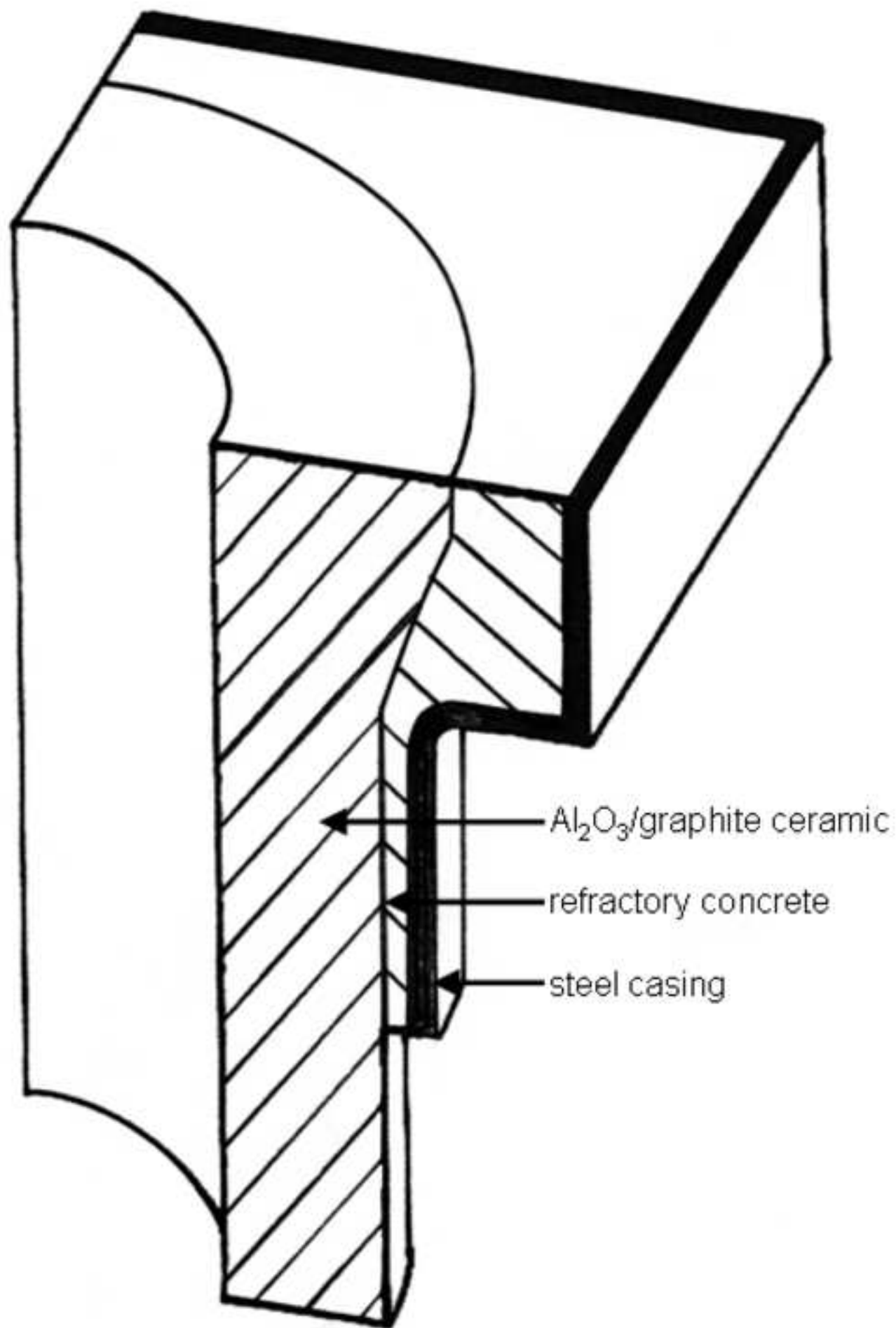
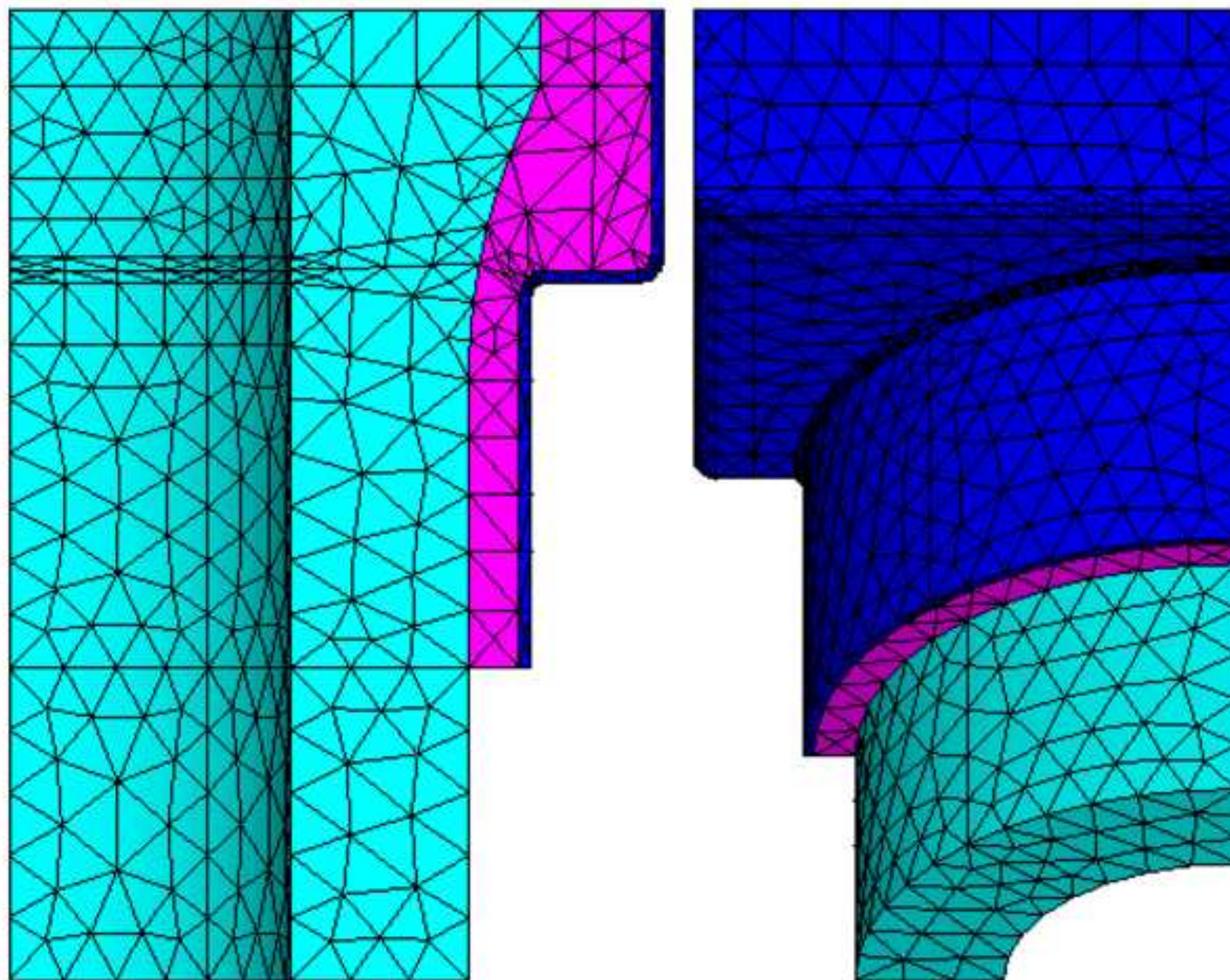



Figure
[Click here to download high resolution image](#)




Figure

[Click here to download high resolution image](#)



 Al₂O₃/graphite ceramic

 refractory concrete


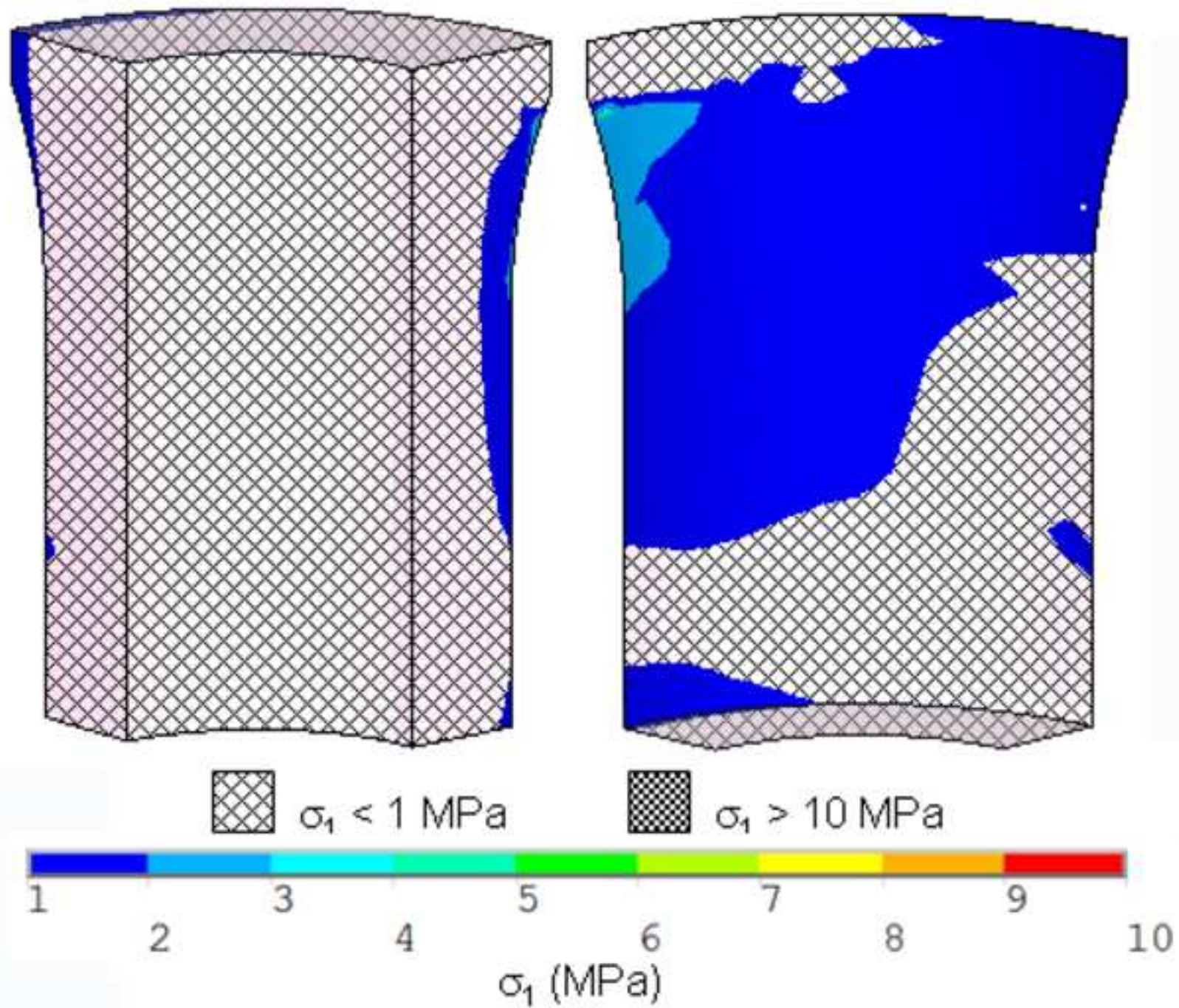
 steel casing

Figure
[Click here to download high resolution image](#)



Figure

[Click here to download high resolution image](#)

